A Solid-State ^{39}K and ^{13}C NMR Study of Polymeric Potassium Metallocenes

Cory M. Widdifield and Robert W. Schurko*

Department of Chemistry and Biochemistry, University of Windsor, Windsor, Ontario, Canada N9B 3P4

Received: February 18, 2005

The quadrupolar Carr−Purcell Meiboom−Gill (QCPMG) and double frequency sweep (DFS)/QCPMG pulse sequences are applied in order to acquire the first solid-state ^{39}K NMR spectra of organometallic complexes, the polymeric main group metallocenes cyclopentadienyl potassium (CpK) and pentamethylcyclopentadienyl potassium (Cp*K). Piecewise QCPMG NMR techniques are used to acquire a high S/N ^{39}K spectrum of the broad central transition of Cp*K, which is ca. 200 kHz in breadth. Analytical and numerical simulations indicate that there is a significant quadrupolar interaction present at both potassium nuclei ($C_Q(^{39}K) = 2.55(6)/2.67(8)$ MHz and 4.69(8) MHz for CpK (static/MAS) and Cp*K, respectively). Experimental quadrupolar asymmetry parameters suggest that both structures are bent about the potassium atoms ($\eta_Q(^{39}K) = 0.28(3)/0.29(3)$ for CpK (static/MAS) and $\eta_Q(^{39}K) = 0.30(3)$ for Cp*K). Variable-temperature (VT) ^{39}K NMR experiments on CpK elucidate temperature-dependent changes in quadrupolar parameters which can be rationalized in terms of alterations of bond distances and angles with temperature. ^{13}C CP/MAS NMR experiments are conducted upon both samples to quantify the carbon chemical shielding anisotropy (CSA) at the Cp′ ring carbon atoms. Ab initio carbon CSA and ^{39}K electric-field gradient (EFG) and CSA calculations are conducted and discussed for the CpK complex, in order to correlate the experimental NMR parameters with molecular structure in CpK and Cp*K. ^{39}K DFS/QCPMG and ^{13}C CP/MAS experiments prove invaluable for probing molecular structure, temperature-dependent structural changes, and the presence of impurities in these systems.

Introduction

Cyclopentadienyl−alkali metal complexes are polymeric organometallic compounds of the form $[Cp'M]_n$, (herein referred to as Cp′M), where M is an alkali metal and Cp′ is a cyclopentadienyl anion of the form $C_5R_5^-$ or $C_5R_xH_{5-x}^-$, with R = H, Me, *i*Pr, etc. These metallocenes have been of significant interest for over a century, due to their fascinating structural types, utility as starting reagents and roles in monomeric anion chemistry.[1,2] While the synthesis and isolation of cyclopentadienyl potassium (CpK) was first reported by Thiele in 1901,[3] structural characterization of Cp′M complexes did not commence until the 1950s: early NMR[4,5] and IR[6] investigations revealed their highly ionic nature and the η^5-bonding interaction between the aromatic π-systems and the alkali metal.

In addition to being only occasionally soluble in polar solvents, Cp′M complexes are rarely soluble in nonpolar and noncoordinating solvents. When certain Cp′M compounds are recrystallized from polar solvents, the solid-state structure often changes from unsolvated linear polymers to solvated linear polymers or monomers with markedly different structures.[1] Crystal structures have been determined for a number of linear potassium-containing solvate polymers, including (TMS)CpK,[7] (*t*BuNHSi)CpK·THP,[8] Cp*K·(pyridine)$_2$ (Cp* = C_5Me_5),[9] and CpK·Et_2O.[10] Unfortunately, the structures of numerous Cp′M complexes (e.g., CpLi, CpNa, Cp*Na, CpK, Cp*K, etc.) cannot be determined by single-crystal X-ray diffraction techniques as they can be isolated only as microcrystalline powders. Recently, synchrotron powder X-ray diffraction experiments, in combination with Rietveld analyses,[11] have been utilized to probe the structures of microcrystalline Cp′M polymers, including CpLi, CpNa, and CpK[12] as well as Cp*Li[13] and Cp*Na.[14]

The Cp′M polymers are extremely reactive and sensitive to contact with air and moisture. As a result, when used as starting materials for organometallic synthesis, there are often disordered impurity phases which cannot be identified by powder X-ray diffraction techniques, which speaks to the limitation of such techniques for their accurate structural characterization. Solid-state NMR experiments, including those from the perspective of the central metal nucleus, have proven to be an ideal tool for characterizing alkali-metal metallocenes, including those in noncrystalline solids. Solid-state NMR studies of metal nuclei in polymeric metallocenes include a ^{7}Li NMR study of lithium metallocenes and other organometallic complexes,[15] as well as ^{23}Na NMR studies of CpNa-TMEDA,[16] an assortment of organosodium complexes,[17] and a variety of Cp′Na complexes.[18]

Potassium has three NMR active isotopes, ^{39}K, ^{40}K, and ^{41}K, all of which are quadrupolar nuclei (nuclear spin, $I > {}^1/_2$): ^{39}K and ^{41}K are spin-$^3/_2$ nuclei, while ^{40}K is a spin-4 nucleus. ^{39}K is the most receptive NMR nucleus of the trio, largely because of its high natural abundance (93.1%) and relatively small nuclear quadrupole moment, Q (accepted values range from 0.055 to 0.11×10^{-28} m^2).[19−22] However, ^{39}K has a very small magnetogyric ratio, γ, relative to nuclei like ^{1}H and ^{13}C, making the acquisition of high-quality solid-state ^{39}K NMR spectra a challenging endeavor.[23] Even more challenging is the acquisition of solid-state ^{39}K NMR spectra of potassium nuclides within nonspherically symmetric electronic environments, which is the case for systems such as CpK and Cp*K. In such systems, significant electric field gradients (EFGs) often lead to large quadrupolar interactions which can broaden the single quantum transitions of NMR powder patterns to such a degree that they

* To whom correspondence should be addressed. Phone: (519) 253-3000 x3548. Fax: (519) 973-7098. E-mail: rschurko@uwindsor.ca.

10.1021/jp058059l CCC: $30.25
Published on Web 07/19/2005

SCHEME 1: (a) QCPMG and (b) DFS/QCPMG Pulse Sequences[a]

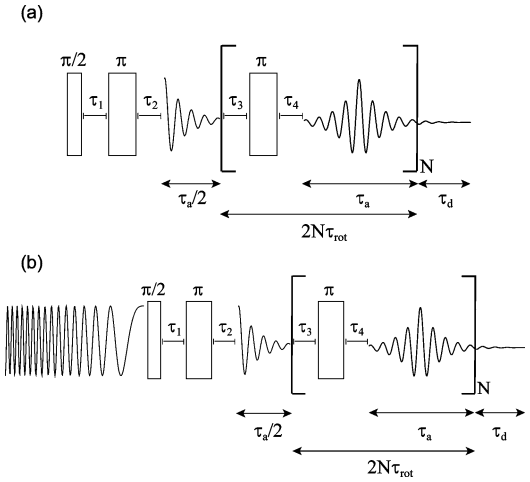

[a] Parameter symbols and definitions are outlined in the Experimental Section.

are undetectable via conventional NMR experiments or at standard magnetic field strengths.[24−26]

Due to the prominence of potassium in a variety of inorganic complexes, biological systems, and technologically relevant materials, ^{39}K NMR experiments have been conducted on many solid systems. Early ^{39}K NMR experiments were used to measure Knight shifts in potassium metal and potassium-containing alloys[27,28] and chemical shifts in solid potassium halides.[20] The combination of spin−echo sequences and higher magnetic field strengths enabled comprehensive ^{39}K NMR studies on a variety of potassium-containing microcrystalline powders.[29,30] Those initial studies led to further research using ^{39}K NMR to probe a variety of systems,[31] including hydrated K^+ ions in smectites,[32] potassium ions in buckminsterfullerides,[21,33] and alkali metal superoxides.[34] Recently, ^{39}K NMR has been used in the study of biological solids,[35] including a high-field study of K^+ ions in G-quadruplex structures.[36]

Thus, even though the rapid acquisition of solid-state ^{39}K NMR spectra would be indispensable in a number of areas, published ^{39}K NMR experiments on nonsymmetric potassium sites remain uncommon. Recently, the quadrupolar Carr−Purcell Meiboom−Gill (QCPMG) pulse sequence was introduced as a method of enhancing the signal-to-noise (S/N) ratio by up to two orders of magnitude in the NMR spectra of half-integer quadrupolar nuclei (Scheme 1a).[37,38] QCPMG NMR experiments have been performed on a variety of inorganic compounds,[38] organic hydrochloride salts (^{35}Cl NMR),[39] biological solids (^{25}Mg and ^{67}Zn NMR),[40,41] and Cp_2Mg (^{25}Mg NMR).[42] The QCPMG sequence has also been used for the detection of the direct dimension in the MQMAS-QCPMG NMR experiment[43] and has been coupled with the double-frequency sweep (DFS)[44,45] and rotor-assisted population transfer (RAPT)[46] pulse sequences for further signal enhancements.[47]

In this paper, we present the first solid-state ^{39}K NMR spectra of organometallic complexes: CpK and pentamethylcyclopentadienyl potassium, Cp*K. The DFS/QCPMG pulse sequence (Scheme 1b) is applied at a standard external magnetic field strength (B_0 = 9.4 T; $\nu_0(^{39}K)$ = 18.65 MHz) to obtain high S/N ^{39}K NMR spectra of very broad central-transition powder patterns. The spectra are simulated to obtain the isotropic chemical shift, $\delta_{iso}(^{39}K)$, the nuclear quadrupolar coupling constant, $C_Q(^{39}K)$, and the quadrupolar asymmetry parameter, $\eta_Q(^{39}K)$. Variable-temperature (VT) ^{39}K NMR experiments are conducted to monitor changes in NMR parameters and molecular structure as a function of temperature. ^{13}C CP/MAS NMR experiments are used to measure the carbon chemical shielding (CS) tensors. Theoretical calculations of ^{39}K EFG tensors and potassium and carbon CS tensors are utilized to correlate NMR parameters to molecular structure. The above techniques support the proposed solid-state structure of CpK and qualitatively predict the structure of Cp*K, while also showing utility as a practical probe of sample purity.

Experimental Section

Syntheses of C_5H_5K (CpK) and $C_{10}H_{15}K$ (Cp*K). Reagents were handled under a nitrogen atmosphere, and all reactions were conducted using a Schlenk line. The syntheses of CpK[48] and Cp*K[49] were based upon those in the literature. Purity of both samples was confirmed by solid-state ^{13}C CP/MAS NMR[5,9] (vide infra) and powder X-ray diffraction[12,50] (see Supporting Information, Figures S1−S2) experiments.

Solid-State NMR. All samples were ground into fine powders under nitrogen atmosphere and packed into 4 mm (for ^{13}C CP/MAS and ^{39}K MAS NMR experiments) and 5 mm (for ^{39}K static experiments) outer diameter (o.d.) zirconium oxide rotors. All rotors were sealed with airtight caps. Solid-state ^{13}C and ^{39}K NMR spectra were obtained using a Varian Infinity Plus NMR spectrometer with an Oxford 9.4 T (^{1}H = 400 MHz) wide-bore magnet at resonance frequencies of $\nu_0(^{13}C)$ = 100.52 MHz and $\nu_0(^{39}K)$ = 18.65 MHz. Central-transition (CT) selective pulses utilized for ^{39}K experiments are equal to the nonselective solution pulse widths scaled by a factor of $(I + 1/2)^{-1}$. For all ^{39}K NMR experiments, tuning and matching the probe circuit was achieved through the use of a Varian/Chemagnetics low-gamma tuning box. A Varian/Chemagnetics 4 mm double-resonance MAS probe was used for all MAS experiments, and a Varian/Chemagnetics 5 mm double-resonance static wide-line probe was used for all static ^{39}K NMR experiments.

^{13}C chemical shifts were referenced to TMS (δ_{iso} = 0.0 ppm) by using the high-frequency peak of adamantane as a secondary reference (δ_{iso} = 38.57 ppm). All ^{39}K chemical shifts were referenced to a saturated solution of KBr (δ_{iso} = 0.0 ppm). For all ^{13}C NMR experiments, the experimental pulse delay used was 5.0 s. For ^{39}K NMR experiments, calibrated pulse delays utilized were 3.0−6.0 and 0.3 s, for CpK and Cp*K, respectively. Variable-temperature (VT) NMR experiments were conducted at temperatures ranging from −120 °C to 60 °C.

^{13}C CP/MAS NMR. ^{13}C CP/MAS NMR experiments on Cp*K were optimized using a $\pi/2$ proton pulse width of 6.75 μs ($\nu_1(^1H)$ = 37.0 kHz), a spectral width of 40 kHz and a contact time of 13 ms. The number of transients collected for each of these experiments (at ν_{rot} = 2.0 kHz and 2.7 kHz) was 48. For CpK, all parameters are the same as above, except that a proton $\pi/2$ pulse width of 5.5 μs ($\nu_1(^1H)$ = 45.5 kHz) was used, 20 transients were collected in each experiment, and ν_{rot} = 2.3 kHz and 3.0 kHz.

^{39}K QCPMG NMR of CpK. All ^{39}K NMR experiments were conducted using variations of the QCPMG pulse sequence, due to the insensitivity of the ^{39}K nucleus.[37] For static experiments, a CT selective $\pi/2$ pulse width of 2.75 μs ($\nu_1(^{39}K)$ = 45.4 kHz), a spectral width of 150 kHz, and a recycle delay of 5.0 s were used. 18 000 acquisitions were collected to achieve reasonable S/N. Interpulse and interacquisition delays τ_1, τ_2, τ_3, and τ_4 were all set to 60 μs. 57 Meiboom−Gill (MG) loops (each loop represents one system response echo and was set equal to 70

points) were acquired, and after the application of a Fourier transform (FT), each QCPMG spikelet was separated by 2143 Hz.

For the MAS-QCPMG experiment, the number of MG loops and echo size were set equal to 40 and 100, respectively and 18 496 transients were acquired. A CT-selective $\pi/2$ pulse of 2.5 μs ($\nu_1(^{39}K) = 50$ kHz), a recycle delay of 3.0 s, and a spectral width of 80 kHz were applied. The MAS-QCPMG pulse sequence requires one to pay special attention regarding the acquisition of rotor-synchronized data: (i) the initial half-echo acquisition is synchronized in the usual MAS-echo manner ($\tau_1 + {}^1/_2\pi = \tau_{rot}$) and (ii) the $[\tau_3\text{-}\pi\text{-}\tau_4\text{-}\tau_a]_N$ portion of the pulse sequence must be set equal to $2N\tau_{rot}$.[51] For this experiment, $\tau_{rot} = 55.56$ μs, resulting in $\tau_1 = \tau_2 = 55.56$ μs and $\tau_3 = \tau_4 = 205.8$ μs.

^{39}K QCPMG NMR of Cp*K. For ^{39}K NMR experiments on Cp*K, the QCPMG pulse sequence was used in a fashion similar to that of the CpK experiments; however, due to the large width of the CT powder pattern (vide infra), the spectrum was acquired in a piecewise fashion using transmitter frequencies of $\nu = 18.71$, 18.65, 18.59, and 18.53 MHz. These four spectra were combined in the frequency domain using co-addition[52−54] and skyline[41] methods. For each piece, a $\pi/2$ pulse width of 2.25 μs ($\nu_1(^{39}K) = 55.6$ kHz) was used, 99 008 transients were acquired, and a spectral width of 150 kHz was employed. All other QCPMG parameters were the same as the static CpK experiment, except that $\tau_1 = \tau_2 = \tau_3 = \tau_4 = 70$ μs.

^{39}K DFS/QCPMG NMR of CpK. The DFS/QCPMG pulse sequence was optimized and run as previously described.[47] All significant QCPMG parameters were kept the same as those in the static ^{39}K QCPMG NMR experiment on CpK. 800 transients were acquired to build an acceptable ratio of S/N in the VT experiments, and 18 000 were acquired in the static experiments. Sweeps began 1.40 MHz and ended 0.15 MHz from the center of gravity of the CT. These sweeps occurred over a period of 850 μs and were divided into 2720 steps, translating into a sweep rate of $\lambda = 1470.6$ MHz/s and a sweep adiabaticity ($A = \nu_1^2/\lambda$) of 0.351.

Spectral Simulations. ^{39}K EFG parameters were determined using both analytical and numerical simulation methods. All experimental spectra were simulated using the analytical simulation package WSOLIDS, which was developed by K. Eichele in R. E. Wasylishen's laboratory at Dalhousie University. WSOLIDS incorporates the space-tiling method of Alderman and co-workers to generate frequency domain solid-state NMR spectra.[55] Numerical simulations were carried out using the SIMPSON simulation package.[56] All SIMPSON simulations were done via the *direct* method of powder averaging using the *zcw4180* crystal file provided with the package, the start and detect operators were set to I_{1z} and I_{1c}, respectively, and the number of gamma angles was set to 20. Error bounds were determined through bidirectional variation of individual NMR parameters, and best-fit spectra were obtained by comparison of root-mean-square difference spectra.

Ab Initio Calculations. The atomic coordinates of CpK were taken from the refined structure obtained from powder XRD.[12] Calculations were carried out on relatively small CpK clusters ($Cp_2K^-/Cp_2K_3^+/Cp_3K_3/Cp_4K_3^-/Cp_4K_4$) (see Supporting Information, Tables S1 and S2) using two Dell Precision workstations running Red Hat Linux. Gaussian 98[57] and Gaussian 03[58] calculations employed either restricted Hartree−Fock (RHF) or hybrid density functional theory (Becke's three parameter hybrid functional using the LYP correlation functional, B3LYP),[59,60] using several standard polarized double-ζ and triple-ζ basis sets provided with the Gaussian software packages (6-31G**/6-311G**/6-311+G**/6-311++G**). Selected calculations used a well-tempered basis set (WTBS) on the potassium atom(s).[61−63] The ^{39}K quadrupolar coupling constant was converted from atomic units into Hz[64,65] by utilizing the formula $C_Q = (eV_{33}Q/h) \times 9.71\,736 \times 10^{21}$ V m^{-2}, where $Q(^{39}K) = 0.055 \times 10^{-28}$ m^2,[20] $e = 1.602\,188 \times 10^{-19}$ C, $h = 6.626\,075\,5 \times 10^{-34}$ J s, and V_{33} is the largest principal component of the EFG tensor. Potassium CS tensors were calculated using the gauge-including atomic orbitals (GIAO) method[66,67] and referenced against the theoretical isotropic shift ($\delta_{iso} = 0.0$ ppm) of $K(OH_2)_6^+$. The absolute potassium CS of $K(OH_2)_6^+$ was calculated from a structure that was geometry-optimized using the same methodology/basis set combination (see Tables S3-(a−p) of the Supporting Information for optimized structures). Embedded cluster molecular orbital (ECMO) calculations used point charges generated from crystallographically determined atomic coordinates in a 20 Å sphere about a central potassium atom both with (2794 point charges) and without (1521 point charges) proton point charges. Standard (e.g., K = +1.00) as well as calculated Mulliken charges were used. Using the MOLDEN software package, a z-matrix of an idealized $Cp_2K_3^+$ crystal structure with C_s symmetry was constructed in an effort to model temperature-dependent structural changes. For these calculations only, both SCF = direct and SCF = tight input commands were used (see Table S4 of the Supporting Information for the format of z-matrix used).

Results and Discussion

^{39}K NMR of CpK. QCPMG and DFS/QCPMG pulse sequences (Scheme 1) were applied to acquire high S/N ^{39}K NMR spectra. The DFS pulse sequence offers theoretical signal enhancement proportional to $2I$ (I being the nuclear spin) when dealing with single-crystals[68] and slightly less when dealing with powders. Before applying DFS/QCPMG, a preliminary QCPMG spectrum is acquired in order to estimate the values of C_Q and η_Q (Supporting Information, Figure S3). These parameters (especially C_Q) must be known, as they determine the high- and low-frequency offset bounds of the frequency sweeps. Optimized ^{39}K static NMR spectra of CpK, acquired with the QCPMG and DFS/QCPMG pulse sequences, as well as an analytical simulation of the powder pattern, are shown in Figure 1. When simulating static QCPMG spectra, there are two alternatives: (i) one may match the outer manifold of echo spikelets in the experimental spectrum with a simulated static powder pattern or (ii) the echoes in the QCPMG time-domain may be co-added and processed to produce a powder pattern which is then directly compared to that of a simulation (Figure 1e). Methods (i) and (ii) are similar, as they very closely match the same simulated powder pattern: $C_Q(^{39}K) = 2.55(6)$ MHz, $\eta_Q(^{39}K) = 0.28(3)$, and $\delta_{iso}(^{39}K) = -100(20)$ ppm (potassium CSA is neglected in the simulation, vide infra).

When comparing experimental and simulated powder patterns of Figures 1a−c, there is not an exact match between the experimental and simulated manifolds; however, the discontinuities and shoulders in the experimental powder pattern can be precisely identified, thereby yielding accurate NMR parameters. Possible reasons for the less than perfect agreement include (i) low S/N, (ii) insufficient number of points comprising the spin−echo, and/or (iii) nonuniform excitation of the CT powder pattern.[69−71] The last explanation may be discarded, as the CT-selective $\pi/2$ pulse width used in the DFS/QCPMG and QCPMG experiments was 2.75 μs ($\nu_1(^{39}K) = 45.4$ kHz), well within the acceptable range for uniform excitation of an approximately 55 kHz wide powder pattern.[72]

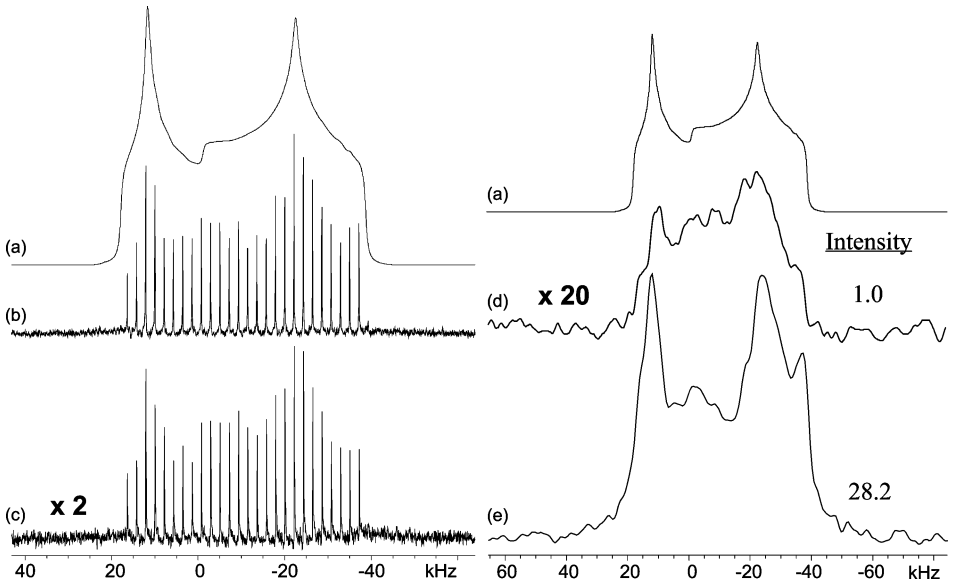

Figure 1. All traces depict static ^{39}K NMR signals of CpK at $\nu_0(^{39}\text{K}) = 18.65$ MHz. (a) Analytical simulation using WSOLIDS; NMR parameters utilized: $C_Q = 2.55(6)$ MHz, $\eta_Q = 0.28(3)$, and $\delta_{iso} = -100(20)$ ppm. For comparison, both (b) DFS/QCPMG and (c) QCPMG spectra were acquired using the same QCPMG parameters, and they clearly depict that the DFS/QCPMG sequence provides higher S/N. Note that the vertical scale of (c) has been increased by a factor of 2. (d−e) Comparison of integrated intensities between (d) the Hahn-echo and (e) the DFS/QCPMG pulse sequences. For this comparison, the vertical scale of (d) was increased by a factor of 20 and given a normalized integrated intensity of 1.0.

Regardless of the minor issues outlined above, the S/N ratios, as well as the system responses isolated from the DFS/QCPMG and QCPMG experiments, are superior to the conventional Hahn-echo experiment (Figure 1d). It is clear that the Hahn-echo sequence is not suitable for solid-state ^{39}K NMR experiments when the electronic environment about the potassium nucleus is not near spherical symmetry. Even after increasing the vertical scale by a factor of 20, the Hahn-echo trace appears nearly void of features, making quantitative NMR analysis very difficult. Overall enhancement, normalized with respect to the integrated intensity of the Hahn-echo experiment, is 28.2 through application of the DFS/QCPMG sequence and 15.2 for the QCPMG pulse sequence. Integrated intensities were obtained by co-adding the CPMG echo trains until a single spin−echo was isolated.[73]

^{39}K MAS NMR experiments on CpK were conducted to confirm quadrupolar parameters using a 4 mm o.d. rotor, which was chosen over the 5 mm rotor due to the relatively high spinning frequency required to separate the spinning sidebands from the CT. A ^{39}K MAS-QCPMG NMR spectrum acquired with a spinning frequency of $\nu_{rot} = 18$ kHz is shown in Figure 2. Spectral simulations using SIMPSON and WSOLIDS reveal $C_Q(^{39}\text{K}) = 2.67(8)$ MHz and $\eta_Q(^{39}\text{K}) = 0.29(3)$, in good agreement with the corresponding static ^{39}K NMR spectra (spinning sidebands are not entirely resolved due to insufficient S/N). The slightly larger C_Q measured in the MAS spectrum is likely the result of frictional sample heating, as opposed to potassium CSA, as the C_Q of alkali metals in unsolvated Cp′M complexes are known to increase with increasing temperature (see ref 18 and VT ^{39}K data below). Analytical simulations including the effect of potassium CSA ($\Omega = 100$ ppm; Supporting Information, Figure S4) suggest that its effect on static ^{39}K NMR spectra is negligible at 9.4 T and that the powder patterns are dominated by the quadrupolar interaction. In addition, theoretical calculations (vide infra) suggest an upper limit to the potassium CSA of about 60 ppm, representing a contribution of less than 2% of the total breadth of the static pattern at 9.4 T. For accurate elucidation of CS tensor parameters, spectral acquisitions at very high fields (e.g., 18.8 T or higher) may be required.

According to powder XRD results, smaller alkali metals such as Li and Na often result in linear chains when they are constituents of Cp′M complexes, whereas the extended structure of CpK is proposed to be a long zigzagging chain. ^{23}Na NMR experiments on linear Cp′Na complexes[18] reveal, in all cases, a near zero value for η_Q, reflecting the axial symmetry of the sodium environments. The nonzero η_Q for CpK is consistent with a zigzagging structure and a nonaxial ground-state electronic environment about the potassium nucleus, thereby supporting the XRD findings.

The low-frequency shift ($\delta_{iso}(^{39}\text{K})$) of CpK with respect to the aqueous standard is similar to that observed for a variety of main-group metallocenes, such as in ^{27}Al NMR spectra of Cp_2Al^+,[74] ^{11}B NMR spectra of Cp_2B^+,[75] and ^{23}Na NMR spectra of Cp′Na complexes.[18] The increase in magnetic shielding results from η^5-coordination of the Cp′ rings to the main group metal. Similar chemical shifts have also been observed for Na^+ and K^+ cations which are coordinated to π-electron systems in solid $Na[BPh_4]$ and $K[BPh_4]$.[76] In addition, although there is a considerable difference between the powder pattern breadths in the ^{39}K NMR spectra of CpK and ^{23}Na NMR spectra of CpNa (55 kHz and 14 kHz, respectively at 9.4 T), their C_Q values are comparable: 2.55 MHz for CpK and 2.97 MHz for CpNa. The increased breadth of the powder pattern in the ^{39}K NMR spectrum results from a combination of (i) low $\nu_0(^{39}\text{K})$ and (ii) much larger EFGs (i.e., larger V_{33}) in CpK (as the eQ for ^{39}K is almost half that of ^{23}Na).

Variable-Temperature (VT) ^{39}K NMR. When acquiring VT ^{39}K NMR data for CpK, conventional Hahn-echo experiments cannot be used as they do not offer enough sensitivity. The QCPMG sequence offers significant S/N enhancement, reducing experimental times to about 5 h per temperature point; however, the DFS/QCPMG pulse sequence is used here as it is even more efficient. By reducing the experimental time to 1 h per temperature point, it reduces wear on the NMR probe and the consumption of cryogens. Thus, even though several steps (outlined earlier) are required to obtain an optimized DFS/QCPMG spectrum, this method is faster than the conventional spin−echo experiment by more than an order of magnitude: it

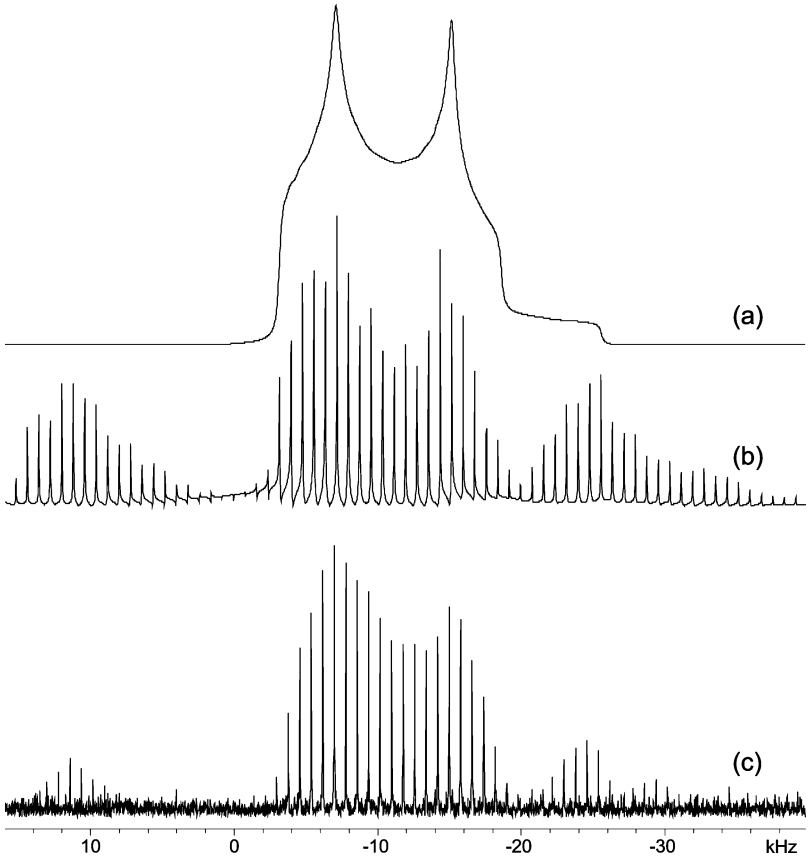

Figure 2. All traces depict ^{39}K MAS NMR signals of CpK at $\nu_0(^{39}\text{K}) = 18.65$ MHz; (a) assumes an infinite spinning frequency, while (b) and (c) were done at $\nu_{rot} = 18$ kHz. (a) Analytical WSOLIDS simulation using the following parameters: $C_Q = 2.67(8)$ MHz, $\eta_Q = 0.29(3)$, and $\delta_{iso} = -75(30)$ ppm. (b) Numerical SIMPSON simulation using the same NMR parameters as (a). (c) Experimental MAS-QCPMG powder pattern of CpK, requiring 18 496 transients (experiment time ~16 h).

TABLE 1: Experimental ^{39}K Chemical Shift and Quadrupolar Parameters

experiment	temp (K)	molecule	C_Q (MHz)	η_Q [a]	δ_{iso} (ppm)[b]
static	293	CpK	2.55(6)	0.28(3)	−100(20)
MAS[c]	293	CpK	2.67(8)	0.29(3)	−75(30)
VT - static	333	CpK	2.60(8)	0.27(3)	−100(30)
VT - static	273	CpK	2.51(8)	0.28(3)	−100(30)
VT - static	213	CpK	2.44(8)	0.29(3)	−100(30)
VT - static	153	CpK	2.35(8)	0.36(3)	−100(30)
static	293	Cp*K	4.69(8)	0.30(3)	−140(40)

[a] Quadrupolar asymmetry parameter, $\eta_Q = (V_{11} - V_{22})/V_{33}$. [b] Isotropic shift, $\delta_{iso} = (\delta_{11} + \delta_{22} + \delta_{33})/3$. [c] MAS rotation frequency, $\nu_{rot} = 18$ kHz.

is estimated that the same set of VT data would take almost a week to gather using the spin−echo sequence.

The number of scans in the VT DFS/QCPMG spectra is decreased with respect to the room-temperature static experiment presented earlier in an effort to reduce experimental time, while still providing a reasonably accurate estimate of changes in quadrupolar parameters with temperature. As the temperature is decreased, the value of C_Q is observed to decrease from 2.60 MHz at +60 °C to 2.35 MHz at −120 °C (Figure 3; Table 1). Similar temperature-dependent behavior was observed for VT ^{23}Na NMR experiments on linear Cp′Na complexes as with decreasing temperature, $C_Q(^{23}\text{Na})$ is observed to decrease. The EFG asymmetry parameter, $\eta_Q(^{39}\text{K})$, is observed to increase from 0.27 to 0.36 as the temperature is decreased from +60 °C to −120 °C. This change is similar to, though more modest than, the temperature-dependent change of $\eta_Q(^{23}\text{Na})$ in the VT ^{23}Na NMR spectra of CpNa·THF. Correlation between observed NMR parameter changes and temperature-dependent structural changes will be addressed in the theoretical section of the discussion.

^{39}K NMR of Cp*K. Initial static ^{39}K NMR experiments on Cp*K revealed that the CT powder pattern exceeded any achievable excitation bandwidth. The small magnetogyric ratio of ^{39}K greatly limits the selective excitation of this extremely broad CT pattern. As QCPMG experiments enhance the rate at which broad powder patterns can be acquired, a piecewise acquisition of the entire powder pattern should be possible. The wide-line NMR experiment employed here is much like the usual NMR experiment but differs such that the final NMR spectrum presented is the sum of several "sub-spectra".[52−54] An initial spectrometer frequency of 18.65 MHz was used due to its proximity to the reference, and then, with the aid of Maple 7,[77] several offset frequencies are theoretically tested to ensure "rectangular-wave" excitation over the entire wide-line spectrum (for more information on the offset selection procedure used, see Supporting Information, Figure S5). Once a reasonable offset frequency has been established, sub-spectra are acquired in both directions until the system response at a particular frequency is significantly reduced; at this point, the lack of response is taken to denote the edge of the central transition. The sub-spectra are then individually subjected to a Fourier transformation and co-added in the frequency domain. Individual slices, as well as the co-added spectrum, are provided in Figure 4a. This methodology is considerably more efficient than the so-called "point-by-point" method,[78] which involves plotting the echo intensity as a function of offset frequency and thereby requires many more data points to be collected. Aside from the co-addition method explained above, it is also possible to

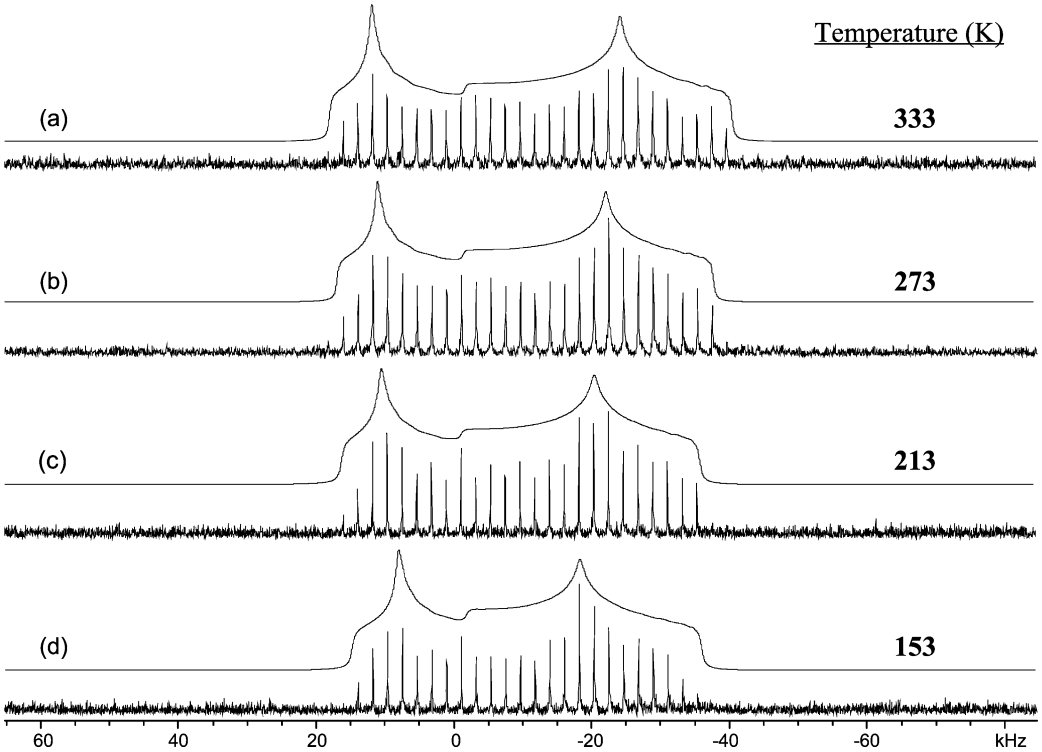

Figure 3. VT ^{39}K NMR spectra of CpK at (a) 333 K, (b) 273 K, (c) 213 K, and (d) 153 K. In all cases, the top trace is the corresponding WSOLIDS analytical simulation of the experimental bottom trace. Simulation parameters are given in Table 1.

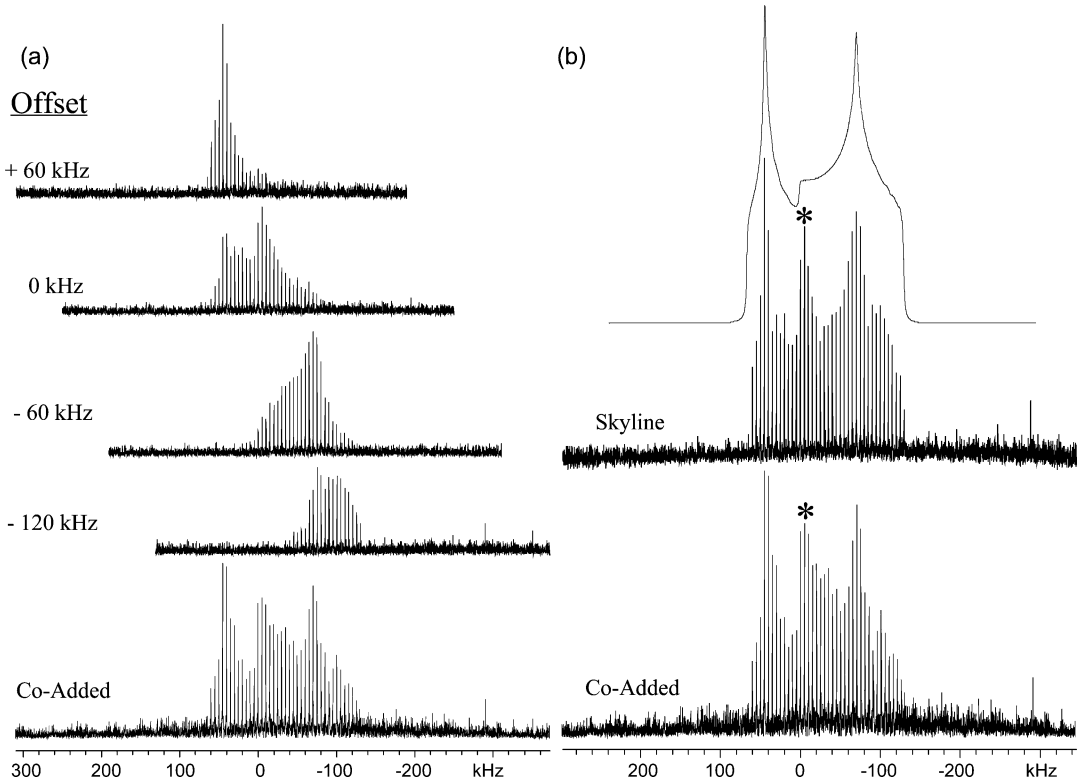

Figure 4. All traces depict static ^{39}K NMR signals of Cp*K. (a) Four static Cp*K ^{39}K NMR sub-spectra, each having a different transmitter offset frequency, are co-added in the frequency domain, producing the bottom trace. (b) WSOLIDS analytical simulation (top trace) using the following parameters: $C_Q = 4.69(8)$ MHz, $\eta_Q = 0.30(3)$, and $\delta_{iso} = -140(40)$ ppm. Corresponding experimental patterns, each composed of four sub-spectra and each sub-spectrum a composite of 99 008 transients, are produced using the skyline (middle trace) and co-addition (bottom trace) processing methods.

produce a skyline projection of the spectra[41] (Figure 4b, middle trace, asterisk denotes an impurity at ca. 0 ppm, which is likely due to the presence of an inorganic potassium salt).

Regardless of the processing method used, the NMR parameters isolated from analytical simulations are very similar to one another: $C_Q(^{39}K) = 4.69(8)$ MHz, $\eta_Q(^{39}K) = 0.30(3)$, and $\delta_{iso}(^{39}K) = -140(40)$ ppm. As it did with CpK, the nonzero η_Q value corresponds to a zigzagging polymeric structure. Additionally, the increased C_Q value for Cp*K relative to CpK can be interpreted as resulting from a decrease in the K−Cp_{cent}

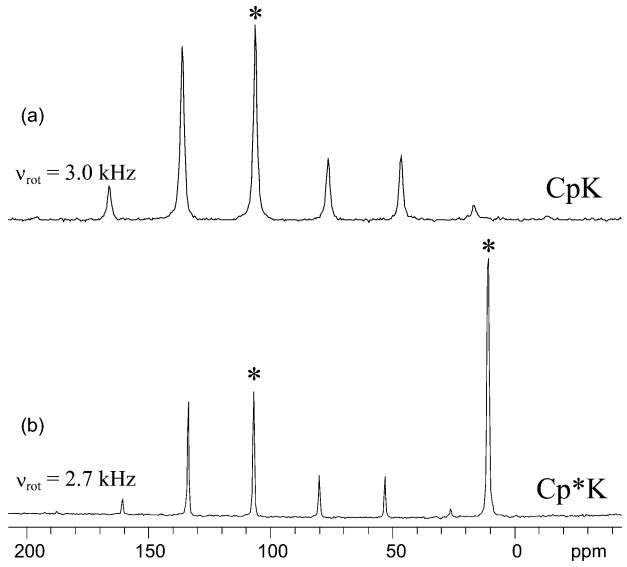

Figure 5. ^{13}C CP/MAS NMR experiments of (a) CpK ($\nu_{rot} = 3.0$ kHz) depict a single, isotropic peak ($\delta_{Cp} = 106.2$ ppm) while similar mechanical rotation conditions (b) ($\nu_{rot} = 2.7$ kHz) show two isotropic peaks ($\delta_{Cp} = 106.8$ ppm; $\delta_{Me} = 11.0$ ppm) for Cp*K.

TABLE 2: Experimental Carbon CS Tensor Parameters

molecule	carbon	δ_{11} (ppm)	δ_{22} (ppm)	δ_{33} (ppm)	δ_{iso} (ppm)[a]	Ω (ppm)[b]	κ [c]
CpK	Cp	146.7	144.3	27.7	106.2	119.0	0.97
Cp*K	Cp	142.6	142.6	35.0	106.8	107.6	1.00
	Me	−	−	−	11.0	−	−

[a] Isotropic shift, $\delta_{iso} = (\delta_{11} + \delta_{22} + \delta_{33})/3$. [b] Span of the CS tensor, $\Omega = \delta_{11} - \delta_{33}$. [c] Skew of the CS tensor, $\kappa = 3(\delta_{22} - \delta_{iso})/\Omega$.

distance, as substitution of the Cp′ ring with alkyl groups has been correlated to a decrease in M−Cp_{cent} distance (see ref 1 and the discussion below dealing with the effects of structural changes on CpK tensor parameters). Solid-state NMR is the only experimental technique for which Cp*K structural information has been elucidated as no structure has been obtained from the available X-ray data.

^{13}C CP/MAS NMR. Carbon-13 CP/MAS NMR experiments were conducted on both CpK and Cp*K in order to measure carbon CS tensors. Presented in Figure 5 are ^{13}C CP/MAS NMR spectra of CpK and Cp*K. In the case of CpK, a single isotropic peak ($\delta_{Cp} = 106.2$ ppm) is observed as the carbon atoms of the Cp ring are undergoing rapid 5-fold reorientations (vide infra). For Cp*K, two isotropic peaks are isolated, one corresponding to the five carbon atoms that comprise the cyclopentadienyl ring ($\delta_{Cp} = 106.8$ ppm), and one belonging to the carbon atoms that are part of the five equivalent methyl groups ($\delta_{Me} = 11.0$ ppm). Herzfeld−Berger analysis[79] was conducted to determine the carbon CS tensors for the aromatic Cp′ carbons. For both CpK and Cp*K, the results clearly show a carbon CS tensor that is very close to being perfectly axially symmetric (i.e., $\delta_{11} \cong \delta_{22}$ according to the standard convention, see Table 2), analogous to the Cp_2Mg[42] and CpNa[18] systems, among others.[74,80,81]

Detection of Impurity Phases via NMR. Polymeric metallocenes are in general very sensitive to air and moisture. Solid-state ^{13}C and ^{39}K NMR can be used to confirm sample purity and potentially identify decomposition products (Supporting Information, Figure S6(a−b)). ^{13}C CP/MAS NMR experiments on a sample of CpK which has been exposed to the atmosphere show no trace of resonances corresponding to Cp ring carbons. The broad peak at ca. 133 ppm corresponds to free cyclopentadiene, while the sharper peaks at 169 and 162 ppm likely correspond to functional groups containing C═O bonds.[82] In addition, ^{39}K NMR spectra reveal a relatively narrow powder pattern, indicating that the potassium is in a completely distinct chemical environment from CpK. If the second-order quadrupolar interaction is taken into account, then the isotropic shift is near 0 ppm, which indicates the presence of a simple potassium salt. The observations of completely different chemical compositions are further supported by powder XRD experiments, which reveal distinct powder patterns for the fresh and exposed samples of CpK (Supporting Information, Figure S6c).

Theoretical Calculations of NMR Tensor Parameters. Calculations were conducted on CpK only, as a refined structure has been proposed from Rietveld analysis of a powder X-ray diffraction pattern.[12] Several calculations used a WTBS on each potassium atom, corresponding to 26 functions describing each of four s-orbitals and 16 functions describing each of two p-orbitals.

^{39}K Quadrupolar Coupling Constant, C_Q. Calculated ^{39}K EFG parameters of basis set/methodology combinations which most closely match the experimental findings for the CpK complex can be found in Table 3 (see Table S5(a) of the Supporting Information for complete data set). When considering calculations that did not employ the WTBS, C_Q values vary between 1.25 and 4.10 MHz, with no one set of calculations approaching the experimental value of 2.55 MHz. Both precision and accuracy are increased when calculations employ a WTBS: C_Q values converge into the 1.38 to 2.65 MHz range; however, there is a corresponding increase in computational time by a factor of 4 to 8. When the WTBS is used on

TABLE 3: Experimental and Theoretical ^{39}K EFG Tensor Parameters for CpK

cluster	method	basis set[a]	V_{11} [b] (au)	V_{22} (au)	V_{33} (au)	$\lvert C_Q \rvert$ [c] (MHz)	η_Q
CpK	exp	static	−	−	−	2.55(6)	0.28(3)
CpK	exp	MAS	−	−	−	2.67(8)	0.29(3)
Cp_2K^-	RHF	6-31G**	−0.0747	−0.1240	0.1987	2.568	0.2481
$Cp_2K_3^+$	RHF	6-31G**	−0.0651	−0.1173	0.1824	2.357	0.2862
Cp_3K_3	RHF	6-31G**	−0.0671	−0.1181	0.1852	2.394	0.2750
$Cp_4K_3^-$	RHF	6-31G**	−0.0694	−0.1191	0.1884	2.435	0.2639
Cp_4K_4	RHF	6-31G**	−0.0685	−0.1185	0.1870	2.417	0.2671
Cp_2K^-	RHF	6-311G**	−0.0753	−0.1298	0.2051	2.651	0.2659
$Cp_2K_3^+$	RHF	6-311G**	−0.0639	−0.1239	0.1878	2.427	0.3192
Cp_3K_3	RHF	6-311G**	−0.0665	−0.1249	0.1915	2.474	0.3049
$Cp_4K_3^-$	RHF	6-311G**	−0.0696	−0.1262	0.1959	2.531	0.2891
Cp_4K_4	RHF	6-311G**	−0.0684	−0.1255	0.1939	2.506	0.2947

[a] Carbon and hydrogen atoms only; WTBS was used on potassium atoms. [b] V_{ii} are the principal components of the EFG tensor, where $|V_{33}| \geq |V_{22}| \geq |V_{11}|$. [c] Calculated C_Q is converted from atomic units into Hz by multiplying V_{33} by $(eQ/h)(9.7177 \times 10^{21}\ \mathrm{V\ m^{-2}})$, where $Q(^{39}\mathrm{K}) = 0.055 \times 10^{-28}\ \mathrm{m^2}$ and where $e = 1.602 \times 10^{-19}$ C.

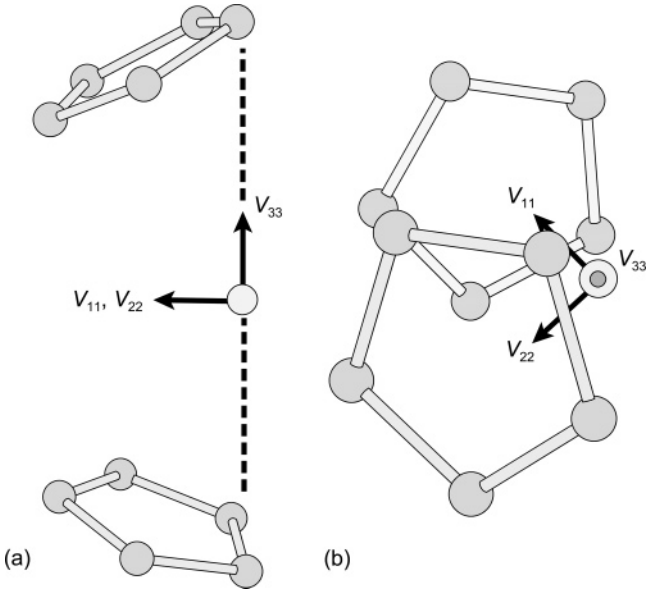

Figure 6. ^{39}K EFG tensor orientations when (a) V_{33} is parallel to the plane of the page and when (b) V_{33} is perpendicular to the plane of the page. Note that the crystallographic *c*-axis is nearly coincident with V_{33}.

the potassium atoms, cluster size does not appear to affect calculated EFG tensor parameters significantly, though cluster size is a significant parameter when WTBSs are not used. Independent of the basis set applied, cluster charge variance along the series +1, 0, −1 results in a steady increase in C_Q. Neither the RHF nor B3LYP method appears to be far superior to the other in predicting the experimental C_Q value when considering all calculations. It is therefore suggested that the calculated values depend most strongly upon (i) molecular charge and, to a lesser extent, (ii) basis set. The RHF method, when used in tandem with anionic clusters and the WTBS basis set on the potassium atoms, has proven to be the best at predicting C_Q.

^{39}K EFG Tensor. As long as certain minimal requirements (polarized triple-ζ basis set on all atoms and $Cp_2K_3^+$ cluster) are satisfied, the ^{39}K EFG tensor orientation is consistent and appears insensitive to any methodology, cluster size/charge or basis set changes. In contrast with sodocene analogues, the major component of the tensor, V_{33}, does not point at the centroid of either of the Cp rings (Figure 6). Rather, V_{33} lies very close to the *c*-axis of the crystallographic unit cell (which has the space group $P\bar{4}2_1c$), which is nearly coincident with the direction of CpK chain propagation. Consequences of these orientations are evident when considering the temperature-dependent changes in the CpK structure (vide infra).

Asymmetry Parameter, η_Q. Regardless of basis set and calculation method, all calculations predict a nonzero value for η_Q, indicating a slight to moderate deviation from axial symmetry about the potassium atom and supporting a zigzagging polymeric structure. Calculations using a polarized double- or triple-ζ basis set on all atoms consistently underestimate η_Q, predicting values between 0.10 and 0.21. Neither the use of larger basis sets of this type nor variations in computational methodology result in close agreement with the experimental η_Q. When a WTBS is used on the potassium atoms, significant improvement is usually observed and is most dramatic when using the RHF method. Cluster charge also appears to be a significant factor in predicting η_Q: as the charge of the cluster changes in the series +1, 0, −1, the calculated η_Q value decreases in a steady manner. The best agreement between experiment and theory is found when employing the RHF method and the WTBS on the potassium atoms, as η_Q is predicted to be between 0.25 and 0.35.

According to the refined XRD structure, every potassium atom is ca. 3.33 to 3.66 Å away from two carbon atoms in neighboring CpK chains, thus it is possible that these nearby chains influence the asymmetry parameter. ECMO calculations were conducted as they may better approximate the electrical environment about the potassium nucleus. Analysis of the results (Table S5a) demonstrate that η_Q values are not approximated any better using this approach, strongly implying that the dominant influences on the ^{39}K EFG tensor are intramolecular. ECMO calculations predict a decrease for the C_Q in all cases and afford a marginally higher correlation between experiment and theory.

Effects of Ring Dynamics and Structural Changes on CpK Tensor Parameters. In an effort to correlate the NMR parameters observed in the ^{13}C CP/MAS NMR and VT ^{39}K NMR experiments with Cp ring dynamics and temperature-dependent structural changes, a computational study was carried out to simulate (i) Cp ring rotation, (ii) lengthening and shortening of the $Cp_{cent}-K$ distance, and (iii) variation in the $Cp_{cent}-K-Cp_{cent}$ angle. Although it may account for minor changes in EFG parameters, the Cp ring "tip angle" (i.e., the angle a plane defined by the Cp ring makes with a vector parallel to the direction of the $Cp_{cent}-K$ bond) was always kept constant at an idealized value of 90°. The atoms of the Cp rings were input as being planar in an effort to reduce computational time (the crystal structure does show a slight deviation from planarity). A single structural parameter (as outlined above) was adjusted in a given set of calculations while holding all other structural parameters fixed, to draw simple qualitative correlations between the adjustable parameter and changes in the appropriate tensor. For all calculations, the $Cp_2K_3^+$ cluster was used with the B3LYP method and 6-311+G** basis set, as this combination provided very good agreement between experiment and theory. This permits comprehensive sets of calculations to be done, while not being overly computationally expensive.

It is quite reasonable to expect rapid Cp ring rotation at room temperature on the time scale of the NMR experiment.[83] Theoretical results presented here strongly support this notion (Figure 7). The barrier associated with ring rotation is slight at about 0.093 kJ/mol (35.4 μHartrees), which is similar to the theoretically determined value for CpNa. Changes in ^{39}K EFG tensor parameters due to rapid Cp ring rotation are negligible, $\Delta C_Q(^{39}K) = 0.0015(1)$ MHz; $\Delta\eta_Q(^{39}K) = 0.004(1)$, and should not account for any discrepancy between experimental and theoretical parameters.

We postulate that the changing ^{39}K quadrupolar parameters in the VT ^{39}K NMR experiments presented above arise from temperature-dependent structural changes in CpK, most likely from temperature-induced alterations in the $Cp_{cent}-K$ bond length and/or a $Cp_{cent}-K-Cp_{cent}$ bond angle. According to the EFG parameters obtained from theoretical modeling, a decrease in C_Q may arise from an increasing $Cp_{cent}-K$ bond distance and/or a decreasing $Cp_{cent}-K-Cp_{cent}$ angle, while an increase in η_Q may be attributed to a decrease in the $Cp_{cent}-K-Cp_{cent}$ angle (Figure 8). The experimentally observed change in η_Q from 0.27 to 0.36, when compared to changes in η_Q that were calculated, shows that the angle variance is slight: the decrease in the $Cp_{cent}-K-Cp_{cent}$ angle from its experimentally determined value is likely in the range 3° to 6° as the temperature is decreased from 333 to 153 K. As V_{33} of the ^{39}K EFG tensor points nearly along the *c*-axis of the unit cell, this likely means

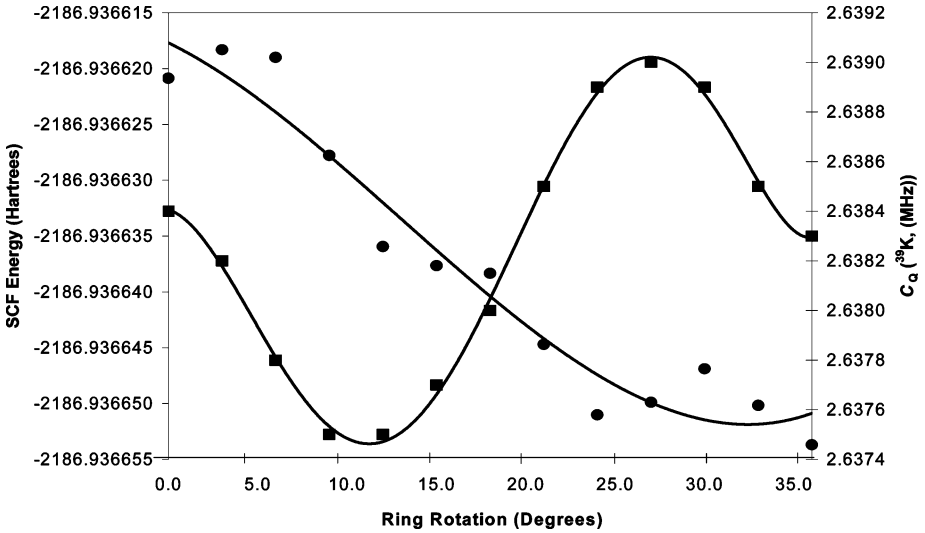

Figure 7. Theoretical calculations indicate the feasibility of rapid Cp ring rotation at ambient temperatures. Results show that C_Q (■) and SCF (●) changes are very slight as the Cp ring is rotated from an eclipsed ($\theta = 0°$) to staggered ($\theta = 36°$) conformation. Calculations were carried out upon an isolated $Cp_2K_3^+$ chain using the B3LYP method and 6-311+G** basis set on all atoms.

TABLE 4: Experimental and Theoretical Potassium Chemical Shielding Tensor Parameters for CpK

cluster	method	basis set	δ_{11} (ppm)	δ_{22} (ppm)	δ_{33} (ppm)	δ_{iso} [a] (ppm)	σ_{iso} (ppm)	Ω[b] (ppm)	κ[c]
CpK	exp	static	–	–	–	−100(20)	–	–	–
CpK	exp	MAS	–	–	–	−75(30)	–	–	–
$Cp_2K_3^+$	RHF	6-31G**	−68.70	−109.66	−110.91	−96.42	1367.32	42.21	−0.94
$Cp_2K_3^+$	RHF	6-31G** [d]	−32.85	−37.43	−43.41	−37.90	1335.18	10.56	0.13
$Cp_2K_3^+$	RHF	6-311G**	−83.61	−127.44	−129.74	−113.59	1365.96	46.13	−0.90
$Cp_2K_3^+$	RHF	6-311G** [d]	−37.48	−45.65	−53.03	−45.38	1336.65	15.56	−0.05
$Cp_2K_3^+$	RHF	6-311+G**	−87.23	−123.24	−126.32	−112.27	1361.85	39.09	−0.84
$Cp_2K_3^+$	RHF	6-311+G** [d]	−67.90	−90.98	−94.91	−84.60	1355.02	27.01	−0.71
$Cp_2K_3^+$	RHF	6-311++G**	−87.96	−121.71	−126.90	−112.19	1360.84	38.94	−0.73
$Cp_2K_3^+$	RHF	6-311++G** [d]	−71.03	−90.38	−91.96	−84.46	1354.92	20.93	−0.85
$Cp_2K_3^+$	B3LYP	6-31G**	−86.45	−131.52	−133.71	−117.23	1364.20	47.26	−0.91
$Cp_2K_3^+$	B3LYP	6-31G** [d]	−27.80	−34.88	−42.09	−34.92	1335.41	14.29	0.01
$Cp_2K_3^+$	B3LYP	6-311G**	−110.90	−139.21	−143.86	−131.32	1344.89	32.96	−0.72
$Cp_2K_3^+$	B3LYP	6-311G** [d]	−30.08	−37.58	−49.31	−38.99	1328.54	19.23	0.22
$Cp_2K_3^+$	B3LYP	6-311+G**	−111.07	−132.93	−138.96	−127.65	1342.51	27.89	−0.57
$Cp_2K_3^+$	B3LYP	6-311+G** [d]	−85.97	−110.79	−115.05	−103.94	1353.15	29.08	−0.71
$Cp_2K_3^+$	B3LYP	6-311++G**	−112.85	−133.64	−143.44	−129.98	1343.05	30.59	−0.36
$Cp_2K_3^+$	B3LYP	6-311++G** [d]	−94.35	−109.16	−114.58	−106.03	1349.91	20.23	−0.46

[a] Isotropic shift, $\delta_{iso} = (\delta_{11} + \delta_{22} + \delta_{33})/3$. [b] Span of the CS tensor, $\Omega = \delta_{11} - \delta_{33}$. [c] Skew of the CS tensor, $\kappa = 3(\delta_{22} - \delta_{iso})/\Omega$. [d] A WTBS on the potassium atom(s).

that as the temperature of the CpK system increases, the polymeric structure of CpK becomes increasingly linear. The temperature-dependent behavior seen here is similar to what was predicted for Cp′Na systems when studied via ^{23}Na NMR, though it is less pronounced in the ^{39}K NMR parameters due to the orientation of the ^{39}K EFG tensor.[18] VT powder X-ray diffraction experiments will be utilized to confirm the proposed models of behavior in a forthcoming study.

Potassium Chemical Shielding. As mentioned earlier, the contribution of potassium CSA to the observed powder patterns does not appear to be particularly significant. In full support of the experimental findings, calculated potassium CSA values (Table 4/Table S5b) predict very minimal CSA-based powder pattern broadening. Theoretical values are relatively close to one another considering the overall breadth of the CpK pattern (9 ppm < Ω < 63 ppm), showing a general independence to the method, basis set, cluster size, and cluster charge used in the calculation. Non-WTBS, RHF calculations with short chains predict the most significant CSA, while WTBS calculations using small basis sets on all other atoms predict the smallest CSA.

Carbon Chemical Shielding. Unlike the ^{39}K NMR experiments, carbon CSA effects can be observed experimentally and theoretically calculated in a relatively accurate manner using any parameter combination presented in this discussion (Table 5/Table S5c). Before accounting for rapid 5-fold ring reorientation, the skew (κ) values are greatly underestimated and span (Ω) values greatly overestimated in all cases. Previous studies upon analogous complexes[18,42,74,80,81] have proven that, for Cp′ ring carbons, (i) the δ_{11} and δ_{22} components of the carbon CS tensor lie nearly parallel to the plane defined by the Cp′ ring and (ii) the Cp′ ring itself undergoes rapid 5-fold reorientations, causing δ_{11} and δ_{22} to be averaged. After accounting for this type of motion, the correlation between experimental and calculated values is substantially higher in all cases, most notably when using the B3LYP method and 6-31G** basis set on carbon and hydrogen atoms.

Conclusions

Solid-state ^{39}K and ^{13}C NMR experiments on polymeric potassium metallocenes, along with theoretically calculated NMR tensors, have proven useful for correlating molecular

TABLE 5: Experimental and Theoretical Carbon Chemical Shielding Parameters for CpK

cluster	method	basis set	δ_{11} (ppm)	δ_{22} (ppm)	δ_{33} (ppm)	δ_{iso} (ppm)	σ_{iso} (ppm)	Ω (ppm)	κ	$(\delta_{11}+\delta_{22})/2$ (ppm)	Ω' [a] (ppm)
CpK	exp	MAS	146.7	144.3	27.7	106.2	–	119.0	0.97	–	–
$Cp_2K_3^+$	RHF	6-31G**	173.34	103.57	5.16	94.03	103.56	168.18	0.17	138.46	133.29
$Cp_2K_3^+$	RHF	6-31G** [b]	172.63	110.37	5.00	96.00	101.59	167.64	0.26	141.50	136.51
$Cp_2K_3^+$	RHF	6-311G**	176.60	101.25	−4.55	91.10	88.31	181.15	0.17	138.92	143.47
$Cp_2K_3^+$	RHF	6-311G** [b]	176.67	99.96	−4.92	90.57	88.84	181.59	0.16	138.32	143.23
$Cp_2K_3^+$	RHF	6-311+G**	178.34	103.23	−4.35	92.41	87.11	182.68	0.18	140.78	145.13
$Cp_2K_3^+$	RHF	6-311+G** [b]	178.23	101.23	−4.69	91.59	87.93	182.92	0.16	139.73	144.42
$Cp_2K_3^+$	RHF	6-311++G**	178.43	103.28	−4.42	92.43	87.09	182.85	0.18	140.86	145.27
$Cp_2K_3^+$	RHF	6-311++G** [b]	178.23	101.51	−4.79	91.70	87.82	183.17	0.16	139.95	144.73
$Cp_2K_3^+$	B3LYP	6-31G**	174.67	109.78	18.64	101.03	96.30	156.03	0.17	142.23	123.59
$Cp_2K_3^+$	B3LYP	6-31G** [b]	173.40	117.02	18.09	102.84	94.49	155.31	0.27	145.21	127.12
$Cp_2K_3^+$	B3LYP	6-311G**	178.94	106.84	5.34	97.04	77.74	173.60	0.17	142.89	137.55
$Cp_2K_3^+$	B3LYP	6-311G** [b]	179.25	103.65	4.76	95.89	78.89	155.31	0.27	145.21	127.12
$Cp_2K_3^+$	B3LYP	6-311+G**	181.24	110.08	6.38	99.23	76.56	174.86	0.19	145.66	139.28
$Cp_2K_3^+$	B3LYP	6-311+G** [b]	180.77	106.33	5.82	97.64	78.15	174.95	0.15	143.55	137.73
$Cp_2K_3^+$	B3LYP	6-311++G**	181.15	109.70	6.37	99.07	76.72	174.78	0.18	145.43	139.06
$Cp_2K_3^+$	B3LYP	6-311++G** [b]	180.62	106.12	6.69	97.81	77.98	173.93	0.14	143.37	136.68

[a] Ω' calculated using averaged value of $(\delta_{11}+\delta_{22})/2$ in place of δ_{11}. [b] A WTBS on the potassium atom(s).

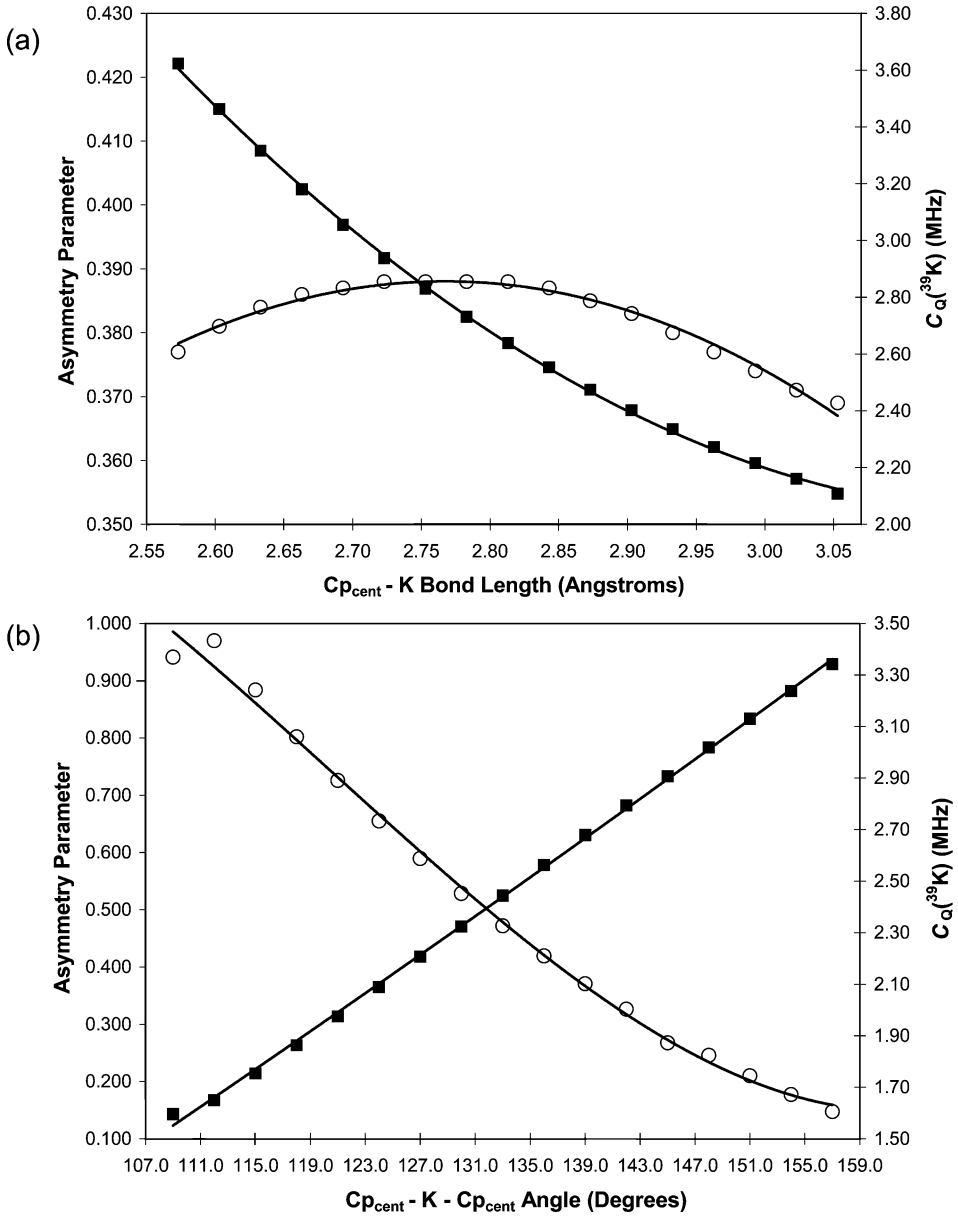

Figure 8. Theoretical calculations showing (a) the change in η_Q (○) and C_Q (■) when the $Cp_{cent}-K$ bond length is modified and (b) the change in η_Q (○) and C_Q (■) when the $Cp_{cent}-K-Cp_{cent}$ angle is modified. Calculations were carried out upon an isolated $Cp_2K_3^+$ chain using the B3LYP method and 6-311+G** basis set on all atoms.

structure to NMR tensor parameters, as well as for observing temperature-dependent structural changes at the molecular level. The application of pulse sequences such as QCPMG and DFS/QCPMG is shown to be invaluable for the acquisition of ^{39}K NMR spectra of CpK and will find much use in the future for acquiring similar spectra of ^{39}K nuclei (along with other low-gamma, half-integer quadrupolar nuclei) in asymmetric environments. A methodology for efficient, uniform, piecewise acquisition of ^{39}K QCPMG NMR spectra for broad powder patterns which exceed the maximum excitable bandwidth is also demonstrated. ^{39}K NMR quadrupolar parameters obtained for CpK support the zigzagging structure proposed from powder XRD data, and similar parameters obtained for Cp*K are used to infer a structure for this hitherto uncharacterized system. The optimized DFS/QCPMG pulse sequence enables the rapid acquisition of VT ^{39}K NMR spectra of CpK, and from these spectra, temperature-dependent structural changes are intimated from changes in the observed values of C_Q and η_Q. ^{13}C CP/MAS NMR experiments on CpK and Cp*K were used to determine carbon CS tensor orientations and confirm the presence of rapid 5-fold Cp ring reorientations. Theoretical calculations on CpK clusters predict ^{39}K NMR parameters relatively well, especially those conducted with large well-tempered basis sets. Clear relationships are shown to exist between the zigzagging nature of the $[Cp'K]_n$ chains and the theoretically calculated ^{39}K EFG tensors (i.e., both the magnitude of principal components and orientation of the EFG tensors). Idealized $Cp_2K_3^+$ clusters were used to see if temperature-dependent structural changes could be correlated to the VT NMR data. It was determined that as temperature is increased, the decreasing value of η_Q and increasing value of C_Q could be correlated to the increasing linearity of the CpK chains. NMR experiments are also useful in identifying the decomposition of CpK and may play a useful role in identifying impurity phases in a variety of potassium-containing materials.

Acknowledgment. This research was funded by Imperial Oil and the Natural Sciences and Engineering Research Council (NSERC − Canada). C.M.W. would like to thank NSERC for an undergraduate scholarship. R.W.S. thanks the Canadian Foundation for Innovation (CFI), the Ontario Innovation Trust (OIT), and the University of Windsor for funding the Solid-State NMR Facility at the University of Windsor. The Centre for Catalysis and Materials Research (CCMR) at the University is thanked for additional funding. We would also like to thank Dr. Ivan Hung for his assistance on this project, Mr. Mathew Willans for assessing the purity of CpK, and Prof. Charles Macdonald (Windsor) for his assistance in both syntheses as well as for the use of his computational resources. We also thank Prof. Robert Dinnebier (Max Planck Institute, Stuttgart) for providing raw powder XRD data on the Cp*K complex.

Supporting Information Available: Figures show powder XRD spectra of both CpK and Cp*K, the initial ^{39}K QCPMG NMR spectrum of CpK, the effect of potassium CSA upon the static ^{39}K NMR spectrum of CpK, a discussion of offset selection for wide-line NMR experiments using Maple 7, and the utility of ^{13}C and ^{39}K NMR in determining sample purity. Tables disclose CpK cluster coordinates used for calculations, calculated SCF energies for various CpK clusters, the theoretical coordinates for the $K(OH_2)_6^+$ complex optimized using a number of parameter combinations, a sample z-matrix used for "dynamic" NMR calculations on CpK, and additional basis set/method combinations that did not appear in the article proper. This material is available free of charge via the Internet at http://pubs.acs.org.

References and Notes

(1) Harder, S. *Coordination Chemistry Reviews* **1998**, *176*, 17.
(2) Weiss, E. *Angewandte Chemie, International Edition in English* **1993**, *32*, 1501.
(3) Thiele, J. *Berichte der Deutschen Chemischen Gesellschaft* **1901**, *34*, 68.
(4) Cox, R. H.; Terry, H. W.; Harrison, L. W. *Journal of the American Chemical Society* **1971**, *93*, 3297.
(5) Fischer, P.; Stadelhofer, J.; Weidlein, J. *Journal of Organometallic Chemistry* **1976**, *116*, 65.
(6) Fritz, H. P.; Schaefer, L. *Chemische Berichte* **1964**, *97*, 1829.
(7) Jutzi, P.; Leffers, W.; Hampel, B.; Pohl, S.; Saak, W. *Angewandte Chemie, International Edition in English* **1987**, *26*, 583.
(8) Schaefer, W. P.; Cotter, W. D.; Bercaw, J. E. *Acta Crystallographica, Section C: Crystal Structure Communications* **1993**, *49*, 1489.
(9) Rabe, G.; Roesky, H. W.; Stalke, D.; Pauer, F.; Sheldrick, G. M. *Journal of Organometallic Chemistry* **1991**, *403*, 11.
(10) Jordan, V.; Behrens, U.; Olbrich, F.; Weiss, E. *Journal of Organometallic Chemistry* **1996**, *517*, 81.
(11) Rietveld, H. M. *Journal of Applied Crystallography* **1969**, *2*, 65.
(12) Dinnebier, R. E.; Behrens, U.; Olbrich, F. *Organometallics* **1997**, *16*, 3855.
(13) Dinnebier, R. E.; Schneider, M.; van Smaalen, S.; Olbrich, F.; Behrens, U. *Acta Crystallographica, Section B: Structural Science* **1999**, *55*, 35.
(14) Tedesco, C.; Dinnebier, R. E.; Olbrich, F.; van Smaalen, S. *Acta Crystallographica, Section B: Structural Science* **2001**, *57*, 673.
(15) Johnels, D.; Boman, A.; Edlund, U. *Magnetic Resonance in Chemistry* **1998**, *36*, S151.
(16) Pietrass, T.; Burkert, P. K. *Inorganica Chimica Acta* **1993**, *207*, 253.
(17) Jost, S.; Gunther, H. *Magnetic Resonance in Chemistry* **2003**, *41*, 373.
(18) Willans, M. J.; Schurko, R. W. *Journal of Physical Chemistry B* **2003**, *107*, 5144.
(19) Kello, V.; Sadlej, A. J. *Chemical Physics Letters* **1998**, *292*, 403.
(20) Sahm, W.; Schwenk, A. *Zeitschrift fur Naturforschung A: Journal of Physical Sciences* **1974**, *29*, 1754.
(21) Sasaki, S.; Matsuda, A.; Chu, C. W. *Physica C: Superconductivity (Amsterdam)* **1998**, *302*, 319.
(22) Grecu, M. N.; Constantinescu, S. *Applied Magnetic Resonance* **1999**, *16*, 373.
(23) Smith, M. E. Recent Progress in Solid-State NMR of Low-Gamma Nuclei. *Annual Reports on NMR Spectroscopy* **2001**, *43*, 121.
(24) Freude, D.; Haase, J. *Quadrupole Effects in Solid-State Nuclear Magnetic Resonance*; Springer-Verlag: Berlin, 1993; Vol. 29.
(25) Vega, A. J. *Quadrupolar Nuclei in Solids*; Wiley: New York, 1996.
(26) Smith, M. E.; van Eck, E. R. H. *Progress in Nuclear Magnetic Resonance Spectroscopy* **1999**, *34*, 159.
(27) Van der Lugt, W.; Knol, J. S. *Physica Status Solidi* **1967**, *23*, K83.
(28) Van der Molen, S. B.; Van der Lugt, W.; Draisma, G. G.; Smit, W. *Physica (Amsterdam)* **1968**, *38*, 275.
(29) Kunwar, A. C.; Turner, G. L.; Oldfield, E. *Journal of Magnetic Resonance* **1986**, *69*, 124.
(30) Bastow, T. J. *Journal of the Chemical Society, Faraday Transactions* **1991**, *87*, 2453.
(31) Bastow, T. J. *Zeitschrift fur Naturforschung A: Journal of Physical Sciences* **1994**, *49*, 320.
(32) Lambert, J. F.; Prost, R.; Smith, M. E. *Clays and Clay Minerals* **1992**, *40*, 253.
(33) Apostol, M. *Journal of Physical Chemistry* **1996**, *100*, 3175.
(34) Krawietz, T. R.; Murray, D. K.; Haw, J. F. *Journal of Physical Chemistry A* **1998**, *102*, 8779.
(35) Wu, G. *Biochemistry and Cell Biology* **1998**, *76*, 429.
(36) Wu, G.; Wong, A.; Gan, Z.; Davis, J. T. *Journal of the American Chemical Society* **2003**, *125*, 7182.
(37) Larsen, F. H.; Jakobsen, H. J.; Ellis, P. D.; Nielsen, N. C. *Journal of Physical Chemistry A* **1997**, *101*, 8597.
(38) Larsen, F. H.; Skibsted, J.; Jakobsen, H. J.; Nielsen, N. C. *Journal of the American Chemical Society* **2000**, *122*, 7080.
(39) Bryce, D. L.; Gee, M.; Wasylishen, R. E. *Journal of Physical Chemistry A* **2001**, *105*, 10413.
(40) Lipton, A. S.; Sears, J. A.; Ellis, P. D. *Journal of Magnetic Resonance* **2001**, *151*, 48.
(41) Lipton, A. S.; Wright, T. A.; Bowman, M. K.; Reger, D. L.; Ellis, P. D. *Journal of the American Chemical Society* **2002**, *124*, 5850.
(42) Hung, I.; Schurko, R. W. *Solid State Nuclear Magnetic Resonance* **2003**, *24*, 78.

(43) Larsen, F. H.; Nielsen, N. C. *Journal of Physical Chemistry A* **1999**, *103*, 10825.

(44) Kentgens, A. P. M.; Verhagen, R. *Chemical Physics Letters* **1999**, *300*, 435.

(45) Iuga, D.; Schafer, H.; Verhagen, R.; Kentgens, A. P. M. *Journal of Magnetic Resonance* **2000**, *147*, 192.

(46) Yao, Z.; Kwak, H. T.; Sakellariou, D.; Emsley, L.; Grandinetti, P. J. *Chemical Physics Letters* **2000**, *327*, 85.

(47) Schurko, R. W.; Hung, I.; Widdifield, C. M. *Chemical Physics Letters* **2003**, *379*, 1.

(48) Wagner, B. O.; Ebel, H. F. *Tetrahedron* **1970**, *26*, 5155.

(49) Schumann, H.; Albrecht, I.; Loebel, J.; Hahn, E.; Hossain, M. B.; Helm, D. *Organometallics* **1986**, *5*, 1296.

(50) Dinnebier, R. E. Private communication.

(51) Larsen, F. H.; Jakobsen, H. J.; Ellis, P. D.; Nielsen, N. C. *Journal of Magnetic Resonance* **1998**, *131*, 144.

(52) Bastow, T. J.; Smith, M. E. *Solid State Nuclear Magnetic Resonance* **1992**, *1*, 165.

(53) Massiot, D.; Farnan, I.; Gautier, N.; Trumeau, D.; Trokiner, A.; Coutures, J. P. *Solid State Nuclear Magnetic Resonance* **1995**, *4*, 241.

(54) Medek, A.; Frydman, V.; Frydman, L. *Journal of Physical Chemistry A* **1999**, *103*, 4830.

(55) Alderman, D. W.; Solum, M. S.; Grant, D. M. *Journal of Chemical Physics* **1986**, *84*, 3717.

(56) Bak, M.; Rasmussen, J. T.; Nielsen, N. C. *Journal of Magnetic Resonance* **2000**, *147*, 296.

(57) Frisch, M. J.; Trucks, G. W.; Schlegel, H. B.; Scuseria, G. E.; Robb, M. A.; Cheeseman, J. R.; Zakrzewski, V. G.; Montgomery, J. A., Jr.; Stratmann, R. E.; Burant, J. C.; Dapprich, S.; Millam, J. M.; Daniels, A. D.; Kudin, K. N.; Strain, M. C.; Farkas, O.; Tomasi, J.; Barone, V.; Cossi, M.; Cammi, R.; Mennucci, B.; Pomelli, C.; Adamo, C.; Clifford, S.; Ochterski, J.; Petersson, G. A.; Ayala, P. Y.; Cui, Q.; Morokuma, K.; Malick, D. K.; Rabuck, A. D.; Raghavachari, K.; Foresman, J. B.; Cioslowski, J.; Ortiz, J. V.; Baboul, A. G.; Stefanov, B. B.; Liu, G.; Liashenko, A.; Piskorz, P.; Komaromi, I.; Gomperts, R.; Martin, R. L.; Fox, D. J.; Keith, T.; Al-Laham, M. A.; Peng, C. Y.; Nanayakkara, A.; Challacombe, M.; Gill, P. M. W.; Johnson, B.; Chen, W.; Wong, M. W.; Andres, J. L.; Gonzalez, C.; Head-Gordon, M.; Replogle, E. S.; Pople, J. A. *Gaussian 98*; revision A.9 ed.; Gaussian, Inc.: Pittsburgh, PA, 1998.

(58) Frisch, M. J.; Trucks, G. W.; Schlegel, H. B.; Scuseria, G. E.; Robb, M. A.; Cheeseman, J. R.; Montgomery, J. A., Jr.; Vreven, T.; Kudin, K. N.; Burant, J. C.; Millam, J. M.; Iyengar, S. S.; Tomasi, J.; Barone, V.; Mennucci, B.; Cossi, M.; Scalmani, G.; Rega, N.; Petersson, G. A.; Nakatsuji, H.; Hada, M.; Ehara, M.; Toyota, K.; Fukuda, R.; Hasegawa, J.; Ishida, M.; Nakajima, T.; Honda, Y.; Kitao, O.; Nakai, H.; Klene, M.; Li, X.; Knox, J. E.; Hratchian, H. P.; Cross, J. B.; Adamo, C.; Jaramillo, J.; Gomperts, R.; Stratmann, R. E.; Yazyev, O.; Austin, A. J.; Cammi, R.; Pomelli, C.; Ochterski, J. W.; Ayala, P. Y.; Morokuma, K.; Voth, G. A.; Salvador, P.; Dannenberg, J. J.; Zakrzewski, V. G.; Dapprich, S.; Daniels, A. D.; Strain, M. C.; Farkas, O.; Malick, D. K.; Rabuck, A. D.; Raghavachari, K.; Foresman, J. B.; Ortiz, J. V.; Cui, Q.; Baboul, A. G.; Clifford, S.; Cioslowski, J.; Stefanov, B. B.; Liu, G.; Liashenko, A.; Piskorz, P.; Komaromi, I.; Martin, R. L.; Fox, D. J.; Keith, T.; Al-Laham, M. A.; Peng, C. Y.; Nanayakkara, A.; Challacombe, M.; Gill, P. M. W.; Johnson, B.; Chen, H.; Wong, M. W.; Gonzalez, C.; Pople, J. A. *Gaussian 03*; revision B.03 ed.; Gaussian, Inc.: Pittsburgh, PA, 2003.

(59) Becke, A. D. *Physical Review A* **1988**, *38*, 3098.

(60) Lee, C.; Yang, W.; Parr, R. G. *Physical Review B* **1988**, *37*, 785.

(61) Huzinaga, S.; Miguel, B. *Chemical Physics Letters* **1990**, *175*, 289.

(62) Huzinaga, S.; Klobukowski, M. *Chemical Physics Letters* **1993**, *212*, 260.

(63) Basis sets were obtained from the Extensible Computational Chemistry Environment Basis Set Database, V., as developed and distributed by the Molecular Science Computing Facility, Environmental and Molecular Sciences Laboratory which is part of the Pacific Northwest Laboratory, P.O. Box 999, Richland, WA 99352, USA, and funded by the U.S. Department of Energy. The Pacific Northwest Laboratory is a multiprogram laboratory operated by Battelle Memorial Institute for the U.S. Department of Energy under Contract DE-AC06-76RLO 1830. Contact David Feller or Karen Schuchardt for further information.

(64) Brown, R. D.; Head-Gordon, M. P. *Molecular Physics* **1987**, *61*, 1183.

(65) Cummins, P. L.; Bacskay, G. B.; Hush, N. S. *Molecular Physics* **1987**, *62*, 193.

(66) Ditchfield, R. *Molecular Physics* **1974**, *27*, 789.

(67) Wolinski, K.; Hinton, J. F.; Pulay, P. *Journal of the American Chemical Society* **1990**, *112*, 8251.

(68) Schafer, H.; Iuga, D.; Verhagen, R.; Kentgens, A. P. M. *Journal of Chemical Physics* **2001**, *114*, 3073.

(69) Dumazy, Y.; Amoureux, J.-P.; Fernandez, C. *Molecular Physics* **1997**, *90*, 959.

(70) Fenzke, D.; Freude, D.; Froehlich, T.; Haase, J. *Chemical Physics Letters* **1984**, *111*, 171.

(71) Man, P. P. *Physical Review B: Condensed Matter* **1995**, *52*, 9418.

(72) Schmidt-Rohr, K.; Spiess, H. W. *Multidimensional Solid-State NMR and Polymers*; Harcourt Brace: Toronto, 1994.

(73) Lefort, R.; Wiench, J. W.; Pruski, M.; Amoureux, J. P. *Journal of Chemical Physics* **2002**, *116*, 2493.

(74) Schurko, R. W.; Hung, I.; Macdonald, C. L. B.; Cowley, A. H. *Journal of the American Chemical Society* **2002**, *124*, 13204.

(75) Schurko, R. W.; Hung, I.; Schauff, S.; Macdonald, C. L. B.; Cowley, A. H. *Journal of Physical Chemistry A* **2002**, *106*, 10096.

(76) Wong, A.; Whitehead, R. D.; Gan, Z.; Wu, G. *Journal of Physical Chemistry A* **2004**, *108*, 10551.

(77) Monagan, M. B.; Geddes, K. O.; Heal, K. M.; Labahn, G.; Vorkoetter, S. M.; McCarron, J.; DeMarco, P. *Maple*, 7 ed.; Waterloo Maple, Inc., 2001.

(78) Zhao, P.; Prasad, S.; Huang, J.; Fitzgerald, J. J.; Shore, J. S. *Journal of Physical Chemistry B* **1999**, *103*, 10617.

(79) Herzfeld, J.; Berger, A. E. *Journal of Chemical Physics* **1980**, *73*, 6021.

(80) Wemmer, D. E.; Ruben, D. J.; Pines, A. *Journal of the American Chemical Society* **1981**, *103*, 28.

(81) Kwon, O.; McKee, M. L. *Journal of Physical Chemistry A* **2001**, *105*, 10133.

(82) Kalinowsky, H.-O.; Berger, S.; Braun, S. *^{13}C NMR Spectroskopie*; Verlag: Stuttgart, 1984.

(83) Orendt, A. M.; Facelli, J. C.; Jiang, Y. J.; Grant, D. M. *Journal of Physical Chemistry A* **1998**, *102*, 7692.